J. Fluid Mech. (1989), *vol.* 209, *pp.* 57–75
Printed in Great Britain

Nonlinear free-surface flow at a two-dimensional bow

By MARK A. GROSENBAUGH† AND RONALD W. YEUNG
Department of Naval Architecture and Offshore Engineering, University of California, Berkeley, CA 94720, USA

(Received 2 May 1988 and in revised form 17 April 1989)

Unsteady free-surface flow at the bow of a steadily moving, two-dimensional body is solved using a modified Eulerian–Lagrangian technique. Lagrangian marker particles are distributed on both the free surface and the far-field boundary. The flow field corresponding to an inviscid, double-body solution is used for the initial condition. Solutions are obtained over a range of Froude numbers for bodies of three different shapes: a vertical step, a faired profile, and a bulbous bow. A transition Froude number exists at which the bow wave begins to overturn and break. The value of the transition Froude number depends on the bow shape. A stagnation point is observed to be present below the free surface during the initial stage of the wave formation. For flows occurring above the transition Froude number, the stagnation point remains trapped below the free surface as the wave overturns. Below the transition Froude number, the stagnation point rises to the surface as the crest of the transient bow wave moves upstream and away from the body.

1. Introduction

Considerable attention has been given in recent years to the study of fluid motion at the bow of a ship. This effort was stimulated by Baba's (1969) observation that there is a significant component of wave resistance associated with the breaking of the bow wave. Since then, much information has been obtained in the form of experimental observations. Theoretical calculations have been successful at explaining linear phenomena but do not account satisfactorily for the nonlinear effects. These include the steepening and overturning of the bow wave which is believed to be a possible source for the necklace of white water that wraps around the bow and the sides of a ship (Mori 1984).

This paper investigates the nonlinear behaviour of the free surface at the bow of a two-dimensional, translating body. A mixed Eulerian–Lagrangian boundary-integral equation method is used to calculate the evolution of the free surface. Because the shape of the free surface is defined by Lagrangian particles, solutions in which the bow wave overturns and breaks are admissible.

Dagan & Tulin (1972) studied two-dimensional, steady flow past a semi-infinite body. Specifically, they derived the small-Froude-number solution, up to second order, of flow past a vertical step. They found that the lowest-order in the asymptotic expansion corresponds to the double-body flow where the free surface is replaced by a rigid wall. This confirms Ogilvie's (1968) assumption that the flow should be linearized about the double-body solution and not the free-stream solution.

† Present address: Department of Ocean Engineering, Woods Hole Oceanographic Institution, Woods Hole, MA 02543, USA.

Vanden-Broeck & Tuck (1977) generalized Dagan & Tulin's formulation to include plane faces of arbitrary angle and derived a method to continue the asymptotic series indefinitely. They found that the asymptotic series has a zero radius of convergence. They were able to sum the series using Shank's transformations, but the resulting free-surface profiles were only piecewise continuous. They argued that the discontinuity is due to the non-uniqueness of the low-Froude-number expansion (Vanden-Broeck, Schwartz & Tuck 1978). Vanden-Broeck & Tuck (1977) concluded that no continuous free-surface profile exists for a bow with a vertical or an oblique flat face. They speculated that the form of the solution is that of an overturning jet.

The possible absence of a nonlinear, steady-state solution in bow flow suggests that a formulation in the time domain is desirable. Our method is based on that of Vinje & Brevig (1981) with modifications made by Lin, Newman & Yue (1984) for handling solid boundaries. Vinje & Brevig, building on the well-known work of Longuet-Higgins & Cokelet (1976), solved the problem of a breaking wave in water of finite depth in terms of the complex potential. Using Cauchy's theorem, they obtained Fredholm integral equations of the second kind for the potential and the stream function. The solution to these equations were then used in the Lagrangian time-stepping scheme to advance the free surface. Baker, Meiron & Orszag (1982), in a similar study, derived integral equations of the second kind by distributing dipoles on the free surface and sources on solid surfaces. A marker-and-cell type model has been used by Miyata, Suzuki & Kajitani (1981) to study nonlinear ship waves.

The novelty in our approach is the treatment of the initial conditions and the far-field closure condition. For closure, we place Lagrangian particles at the nodes of the elements of the far-field boundary. (These are in addition to the Lagrangian particles distributed on the free surface.) We derive evolution equations for the position and the potential of the particles on the far-field boundaries. The evolution equation for the potential is an approximation. In Vinje & Brevig (1981) a closure condition was imposed by assuming that the solution was spatially periodic. In Lin *et al.* (1984), the domain is treated as being closed.

In traditional studies of time-dependent flow past a body, the initial conditions that are specified correspond to an impulsive start from rest. In such formulations, the velocity potential is taken to be zero on the free surface at time $t = 0$. Lin *et al.* (1984) solved for the impulsive motion of a wavemaker using such initial conditions and found that the elevation of the intersection point between the body and the free surface is unbounded. This difficulty can be somewhat remedied by a non-impulsive start as suggested by Roberts (1987). However, we found that numerical implementation of a gentle start-up required a series of small, impulsive accelerations which eventually caused an unbounded rise in the free-surface elevation at the intersection point.

In reality, the free-surface elevation at the bow of a steadily translating ship remains finite for all time. With this in mind, we sought alternative initial conditions, ones that would result in bounded wave elevations. Here, the initial conditions are specified as the steady-state solution for a semi-infinite body with a rigid free-surface condition (i.e. the double-body flow). This corresponds to placing a lid over the free surface and allowing the flow to reach steady state. At $t = 0$, the lid is removed, and the flow is allowed to evolve. An important consequence of this approach is that we have avoided accelerating the body impulsively, and thus avoided an unbounded free-surface elevation.

In §2, we review briefly the boundary-integral formulation used to solve for the

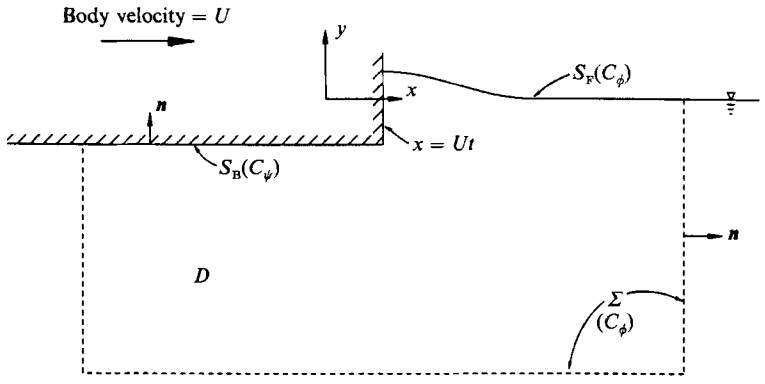

FIGURE 1. Computational domain for flow past a semi-infinite body with a vertical face.

flow field and also review the evolution equations used to advance the free surface. The new far-field boundary conditions and initial conditions are discussed in §3. In §4, we present a sample calculation for the flow around a vertical step and show the self-consistency of the solution method by comparing the increase in fluid energy to the amount of work done on the fluid by the boundaries. Calculations for bodies with different bow shapes and different translational speeds are given in §5 along with a discussion of the results. This is followed by concluding remarks in §6.

2. Mathematical formulation

We formulate the problem of time-dependent, two-dimensional flow past a semi-infinite body having an arbitrary bow shape and a maximum draught of d. As an illustration, we consider a body with vertical face initially located at $x = 0$ and with a bottom, extending from $x = 0$ to $x = -\infty$, at $y = -d$ (see figure 1). The body is assumed to translate with a horizontal velocity U. The fluid domain D is enclosed by the body boundary S_B, the free-surface boundary S_F, and the far-field boundary Σ. The total boundary $S_F \cup S_B \cup \Sigma$ will be referred to as C.

Assuming irrotational flow and incompressible fluid, we describe the absolute motion of the fluid inside the domain by a complex potential $\beta(z,t)$:

$$\beta(z,t) = \phi(z,t) + \mathrm{i}\psi(z,t), \tag{1}$$

where $\phi(z,t)$ is the velocity potential and $\psi(z,t)$ is the stream function. The complex potential is an analytic function of $z = x + \mathrm{i}y$. Thus, Cauchy's integral formula can be used to derive integral equations that relate the variables in the field to the values of $\beta(z,t)$ on the field's boundary.

2.1. *Integral equation and its numerical treatment*

The following is a brief description of the integral-equation formulation. A more complete account is given in Vinje & Brevig (1981). We apply Cauchy's integral formula to the analytic function β, evaluating it at a point z_0 inside the fluid domain:

$$\beta(z_0,t) = \frac{1}{2\pi\mathrm{i}} \int_C \frac{\beta(z,t)}{z - z_0}\,\mathrm{d}z, \quad z_0 \in D. \tag{2}$$

Differentiating (2) with respect to z_0 yields a similar expression that relates the boundary values of β to the complex velocity w inside the fluid domain:

$$w(z_0,t) = \frac{1}{2\pi i}\int_C \frac{\beta(z,t)}{(z-z_0)^2}\,dz, \quad z_0 \in D, \tag{3}$$

where w is given by

$$w(z_0,t) = u(z_0,t) - iv(z_0,t), \tag{4}$$

with u and v being the fluid velocity components in the x- and y-directions respectively.

As is well known in potential theory, if z_0 approaches C, Cauchy's integral formula becomes

$$\beta(z_0,t) = \frac{1}{\alpha i}\int_C \frac{\beta(z,t)}{z-z_0}\,dz, \quad z_0 \in C, \tag{5}$$

where α is the interior angle between the two tangents intersecting locally at z_0. If C is smooth, then $\alpha = \pi$.

We show in the next section that the boundary conditions are mixed. On the free surface and the far-field boundary $S_F \cup \Sigma$ only the potential ϕ is specified, and on the body S_B only the stream function ψ is specified. The portions on which ϕ is given are referred to as C_ϕ; the parts of the boundary on which ψ is given are referred to as C_ψ. The key step in calculating the flow is to determine the unknown portion of β around the boundary. Then we can apply (2) and (3) to calculate the flow everywhere in the fluid domain. Taking the real Re and imaginary Im parts of (5), we obtain

$$\begin{Bmatrix} -\psi(z_0,t) \\ +\phi(z_0,t) \end{Bmatrix} = \begin{Bmatrix} \mathrm{Re} \\ \mathrm{Im} \end{Bmatrix} \left(\frac{1}{\alpha}\int_C \frac{\beta(z,t)}{z-z_0}\,dz \right), \quad z_0 \in \begin{Bmatrix} C_\phi \\ C_\psi \end{Bmatrix}. \tag{6}$$

Equation (6) can be used to determine the unknown ϕ and ψ on C_ψ and C_ϕ respectively at each value of t. The integral equations are Fredholm type of the second kind; the existence and uniqueness of their solutions are well studied.

We seek an approximate solution of the integral equations by dividing the contour C into line segments defined by the nodes z_j and z_{j+1} where $j = 1, \ldots, N$. If $\beta(z)$ is discretized as

$$\beta(z) = \sum_{j=1}^{N} \beta_j \Lambda_j(z), \tag{7}$$

where Λ_j are the 'shape functions' and β_j are the nodal values at z_j, then (6) can be reduced to the following approximate linear system:

$$\begin{Bmatrix} -\psi(z_k) \\ +\phi(z_k) \end{Bmatrix} = \begin{Bmatrix} \mathrm{Re} \\ \mathrm{Im} \end{Bmatrix} \left(\frac{1}{\alpha} \sum_{\substack{j=1 \\ j \neq k}}^{N} \Gamma_{k,j}\beta_j \right), \quad z_0 \in \begin{Bmatrix} C_\phi \\ C_\psi \end{Bmatrix}. \tag{8}$$

The $\Gamma_{k,j}$ are influence coefficients which can be obtained by straightforward integration once $\Lambda_j(z)$ are chosen.

The nodal points at which the boundary conditions are discontinuous (where C_ϕ and C_ψ intersect) require special care. At these points, both the potential and the stream function should be specified (Lin *et al.* 1984). Since both parts of β are known at the intersection points, we remove the equations that correspond to these nodes from the linear system. In the cases that we study in this paper, there are two such points, $S_F \cap S_B$ and $S_F \cap \Sigma$, so we are always solving a system of $(N-2)$ equations

in $(N-2)$ unknowns. The solution to these equations is obtained by Gauss–Seidel iteration. Rapid convergence can be achieved by using the solution from the previous time step as an initial guess.

2.2. *Body and free-surface boundary conditions*

Since the body boundary is a streamline and is translating at a constant velocity U, the stream function on S_B is known for all time and is simply given by

$$\psi(z,t) = U(y+1), \quad z \in S_B. \tag{9}$$

The evolution of the positions and the values of the potential of fluid particles on the free surface S_F is carried out in a manner suggested by Longuet-Higgins & Cokelet (1976). The positions of the fluid particles are integrated in time using the kinematic free-surface boundary condition

$$\frac{Dz}{Dt} = w^* = u + iv, \quad z \in S_F, \tag{10}$$

where the superscript asterisk denotes complex conjugate and D/Dt is the material derivative. The potential ϕ is integrated in time using the dynamic boundary condition

$$\frac{D\phi}{Dt} = \tfrac{1}{2}ww^* - g\eta, \quad z \in S_F, \tag{11}$$

where $y = \eta(x,t)$ is the free-surface elevation and g is the gravitational acceleration.

3. Far-field conditions and initial conditions

The far-field boundary is treated as a material surface whose position changes with time. The positions of fluid particles on this boundary evolve according to the same equation that describes the motion of free-surface particles:

$$\frac{Dz}{Dt} = w^* = u + iv, \quad z \in \Sigma. \tag{12}$$

By Euler's integral, the material derivative of the potential of the particle is given by

$$\frac{D\phi}{Dt} = \tfrac{1}{2}ww^* - gy - \frac{p}{\rho}, \quad z \in \Sigma, \tag{13}$$

where p is the fluid pressure. This equation is the same as (11) except for the extra pressure term. This term vanishes on the free surface but, in general, will not for a submerged particle. A field equation for p can be obtained by taking the divergence of the gradient of (13):

$$\frac{1}{\rho}\nabla^2 p(z,t) = -\tfrac{1}{2}\nabla^2(ww^*), \quad z \in \Sigma. \tag{14}$$

As is well known, the elliptic nature of p implies the necessity of knowing p outside of Σ.

We can avoid having to solve (14) if we know how the pressure of a fluid particle evolves with time. From (13), taking the material derivative of p, we obtain

$$-\frac{1}{\rho}\frac{Dp}{Dt} = \frac{\partial^2\phi}{\partial t^2} + g\frac{\partial\phi}{\partial y} + \frac{D}{Dt}(\tfrac{1}{2}ww^*) + w\frac{\partial w^*}{\partial t}. \tag{15}$$

If the quadratic terms in velocity are neglected, then

$$-\frac{1}{\rho}\frac{\mathrm{D}p}{\mathrm{D}t} \approx \frac{\partial^2\phi}{\partial t^2} + g\frac{\partial\phi}{\partial y}, \tag{16}$$

with error of $O(|z|^{-2})$ for a source-like flow. Further, if the far-field potential could be represented by a linear, time-dependent wave source (Finklestein 1957) located at $\tilde{z} = Ut - ib$ (where b is the distance below the free surface), then the far-field potential may be approximated by

$$\phi(x,y,t) = \frac{\sigma(t)}{2\pi}\log\frac{|z-\tilde{z}|}{|z-\tilde{z}^*|} - \frac{g}{\pi}\mathrm{Re}\int_0^t \sigma(\tau)\,\mathrm{d}\tau \int_0^\infty \frac{\mathrm{d}k}{(gk)^{\frac{1}{2}}} \mathrm{e}^{\mathrm{i}k(z-\tilde{z})}\sin[(gk)^{\frac{1}{2}}(t-\tau)], \tag{17}$$

where $\sigma(t)$ is the source strength at time t and $\tilde{z}^*$ is the location of the image source. It is possible to show that the second term associated with (17) satisfies the right-hand side of (16). Thus, the first term of (17) yields the dominant contribution

$$-\frac{1}{\rho}\frac{\mathrm{D}p}{\mathrm{D}t} \sim O\left(\frac{by}{x^2+y^2}\right) \quad \text{as} \quad z \to \infty. \tag{18}$$

Here, we employ the condition

$$\frac{\mathrm{D}p}{\mathrm{D}t} = 0, \quad z \in \Sigma, \tag{19}$$

with p given for all time by an initial condition at $t = 0$. Equation (19) states that far from the bow, all isobars are material surfaces. This is an approximate condition that becomes exact in the limit as $z \in \Sigma$ goes to ∞. If we place the far-field boundary sufficiently far from the bow of the body, then the right-hand side of (18), which goes as $O(|z|^{-1})$, will be small and have little effect on the calculation. We demonstrate in the next section that the errors in the solution caused by the implementation of (19) appear over time as a drop in the upstream water level. This gives a convenient criterion for selecting the location of the far-field boundary. We simply place Σ far enough away from the bow of the body so that the drop of the upstream water level remains small for all time.

Initial conditions on the free surface and far-field boundary must now be given in terms of the position, the potential, and the pressure. The initial positions of the fluid particles are

$$\eta(x,0) = 0, \quad z \in S_{\mathrm{F}}, \tag{20}$$

$$z = z_0, \quad z \in \Sigma, \tag{21}$$

where z_0 represents the position of the far field at $t = 0$. The initial condition for ϕ on both the free surface and far-field boundary is specified as

$$\phi(z,t) = \phi_0 \quad \text{at} \quad t = 0, \tag{22}$$

where ϕ_0 represents the values of the potential from the *steady-state, double-body* solution ($\partial\phi/\partial y = 0$ at $y = 0$) satisfying (9). A pressure field p^- therefore exists in the fluid at $t = 0^-$ and is given by

$$\frac{p^-}{\rho} = -\tfrac{1}{2}|\nabla\phi_0|^2. \tag{23}$$

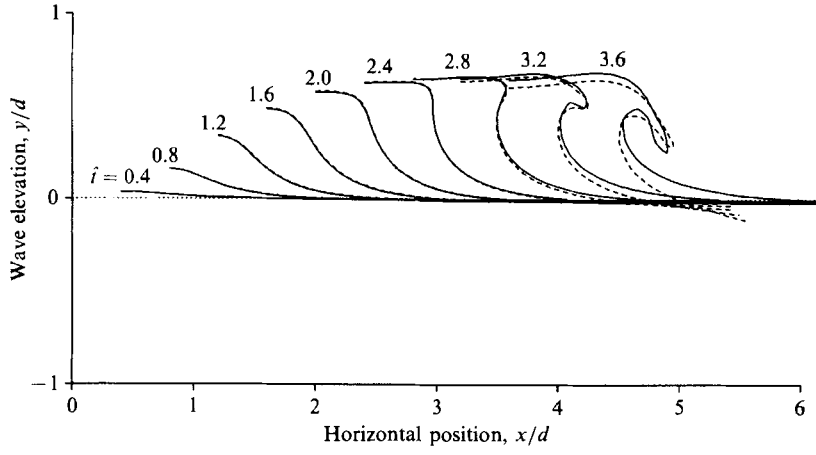

FIGURE 2. Sample calculation of bow-wave evolution for draught Froude number $F_d = 1.0$ and time $\hat{t} = 0$ to 3.6. Case 1 (——): the upstream boundary is located initially 20 units upstream. Case 2 (– – – –): upstream boundary is placed 5.25 units upstream.

At $t = 0^+$, (13) applies, thus

$$\frac{\partial \phi}{\partial t}(z, 0^+) + \tfrac{1}{2}|\nabla \phi_0|^2 + gy + \frac{p(z, 0^+)}{\rho} = 0, \quad z \in D. \tag{24}$$

The requirement that $p(z, 0^+) = 0$ on S_F and the continuity of ϕ at $t = 0$ thus imply that for $z \in D$

$$\frac{\partial \phi}{\partial t}(z, 0^+) = \frac{p^-}{\rho}, \tag{25}$$

$$p(z, 0^+) \equiv p_0 = -\rho g y_0, \tag{26}$$

where p_0 is the initial pressure field that exists at $t = 0^+$. Physically, (22) and (26) represent a sudden removal of the pressure distribution from the free surface.

Thus, using (19), (13) yields the evolution equation of ϕ for a fluid particle on Σ. Equation (8) can then be used to determine ψ and consequently the complex velocity w.

An alternative boundary condition on Σ is to specify $\psi = \psi_0$ for all time, where ψ_0 is the stream function that corresponds to the double-body flow. This condition implies that the net flux into D equals zero. When this was implemented, the shape of the bow wave was found to be similar to that obtained in the present study, but the upstream asymptotic water level fell below the equilibrium waterline (see Grosenbaugh 1987). This occurred as a result of the rise of the wave elevation at the bow and the need to satisfy continuity. By specifying the potential ϕ on Σ and allowing it to evolve with the solution, as we have done in this paper, fluid can accumulate at the bow of the body without having to be offset elsewhere.

4. A test problem and energy conservation

The flow solution for a simple bow geometry was obtained using the formulation described in the previous sections, and the results are shown in figure 2. The evolution of the free surface for $\hat{t} = 0$ to $\hat{t} = 3.6$ is plotted at time intervals of 0.4,

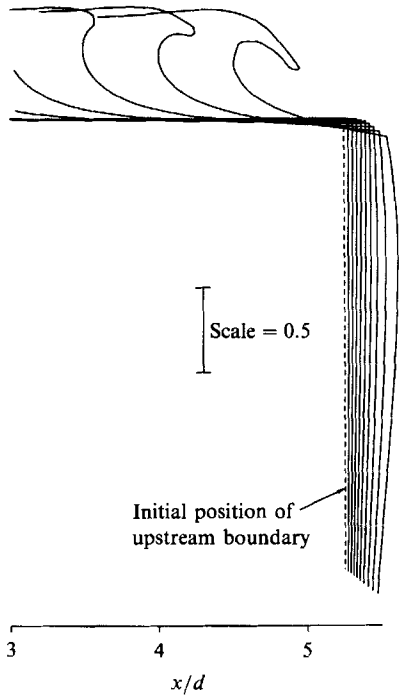

FIGURE 3. Change in position of the upstream, far-field boundary with the approach of the bow wave. Case 2.

where $\hat{t} \equiv t(g/d)^{\frac{1}{2}}$. The draught Froude number, defined as $F_d \equiv U/(gd)^{\frac{1}{2}}$, was equal to 1.0. The evolution equations (10)–(13) were solved using a fourth-order Adams predictor–corrector method with a fourth-order Runge–Kutta algorithm as the starter (Hildebrand 1976). The size of the time step was 0.01. A regridding scheme (Dommermuth & Yue 1986) based on spline fitting was applied every 20 time steps to eliminate a sawtooth instability reported by Longuet-Higgins & Cokelet (1976).

The solid curves in figure 2 correspond to calculations obtained using a fluid domain that extended initially 20 units upstream and downstream and was 20 units deep (Case 1). A test of the robustness of the far-field boundary conditions was made by placing the upstream boundary 5.25 units ahead of the body and repeating the calculations (Case 2). These results are shown in figure 2 by the dashed curves. Differences between the two results are most pronounced when the bow wave, in Case 2, is near the upstream boundary. This is expected because the assumptions implied by (19) are no longer valid. Figure 3 is an expanded view of the Case 2 calculations. The plot shows clearly how the upstream boundary responds to the approach of the body and its bow wave.

It is desirable to apply an accuracy check to the calculations based on energy considerations. A form slightly different from that of John (1949) is used here. We define

$$E(t) = \iint_D (\tfrac{1}{2}\rho|\nabla\phi|^2 + \rho g(y - y_0))\,\mathrm{d}S, \tag{27}$$

which represents a sum of the kinetic energy and the potential energy (relative to the initial configuration of the fluid). We can derive the following relation (see Yeung

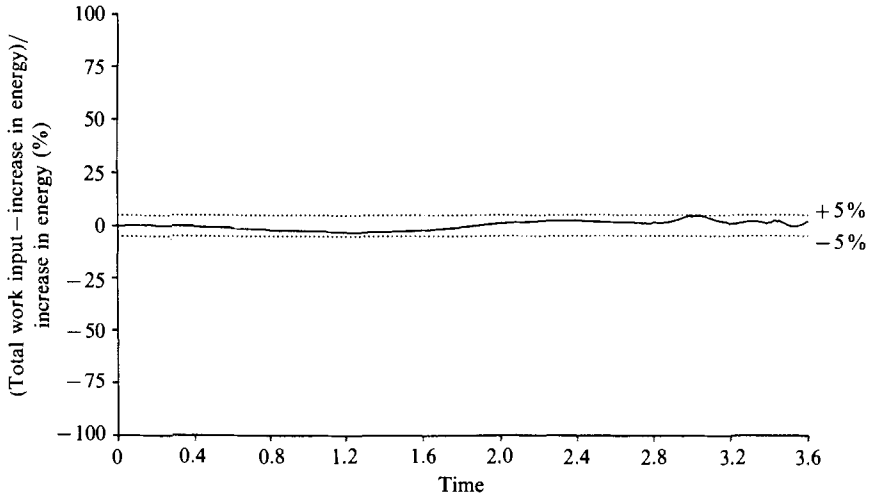

FIGURE 4. The relative difference between the amount of work input to the fluid domain and the increase in energy of the fluid for Case 1 of the test problem (refer to figure 2).

1982) between the amount of work done by the boundaries on the fluid domain and the change in the energy of the fluid:

$$W(t) = \int_C \tfrac{1}{2}\rho\left(\phi\frac{\partial\phi}{\partial n} + g(y-y_0)^2 n_y\right)\mathrm{d}l - E_0, \quad t > 0^+, \tag{28}$$

where E_0 is the value of (27) at time $t = 0^+$ and

$$W(t) = -\int_0^t \mathrm{d}\tau \int_{S_B} (p-p_0)\frac{\partial\phi}{\partial n}\mathrm{d}l. \tag{29}$$

An energy balance calculation was performed on the results obtained from the study of Case 1 (see figure 2). The integrals in (28) and (29) were calculated by trapezoidal integration. The percent difference between the amount of work, given by the left-hand side of (28), and the increase in fluid energy from the initial state, given by the right-hand side of (28), is plotted as a function of time in figure 4. The plot shows that the relative differences for this example were always less than 5%.

5. Results and discussion

We obtained the solution of the bow-flow problem for three different geometries: a vertical step, a body with a rounded stem which will be referred to as a 'faired body', and a body having a protruding or bulbous bow. We now present these results.

The evolution of the free surface near the bow of the vertical step was computed over a range of draught Froude numbers from 0.5 to 1.0 (see figure 5). All results presented here are plotted in a coordinate system that is moving with the body (from left to right). For $F_d = 0.5$ and $F_d = 0.6$, the wave profiles are plotted every 0.8 non-dimensional time units. For $F_d \geqslant 0.7$, they are plotted every 0.4 time units. The size of the time step for all the calculations was 0.01 time units. A time step of 0.02 was used to check the convergence of the results.

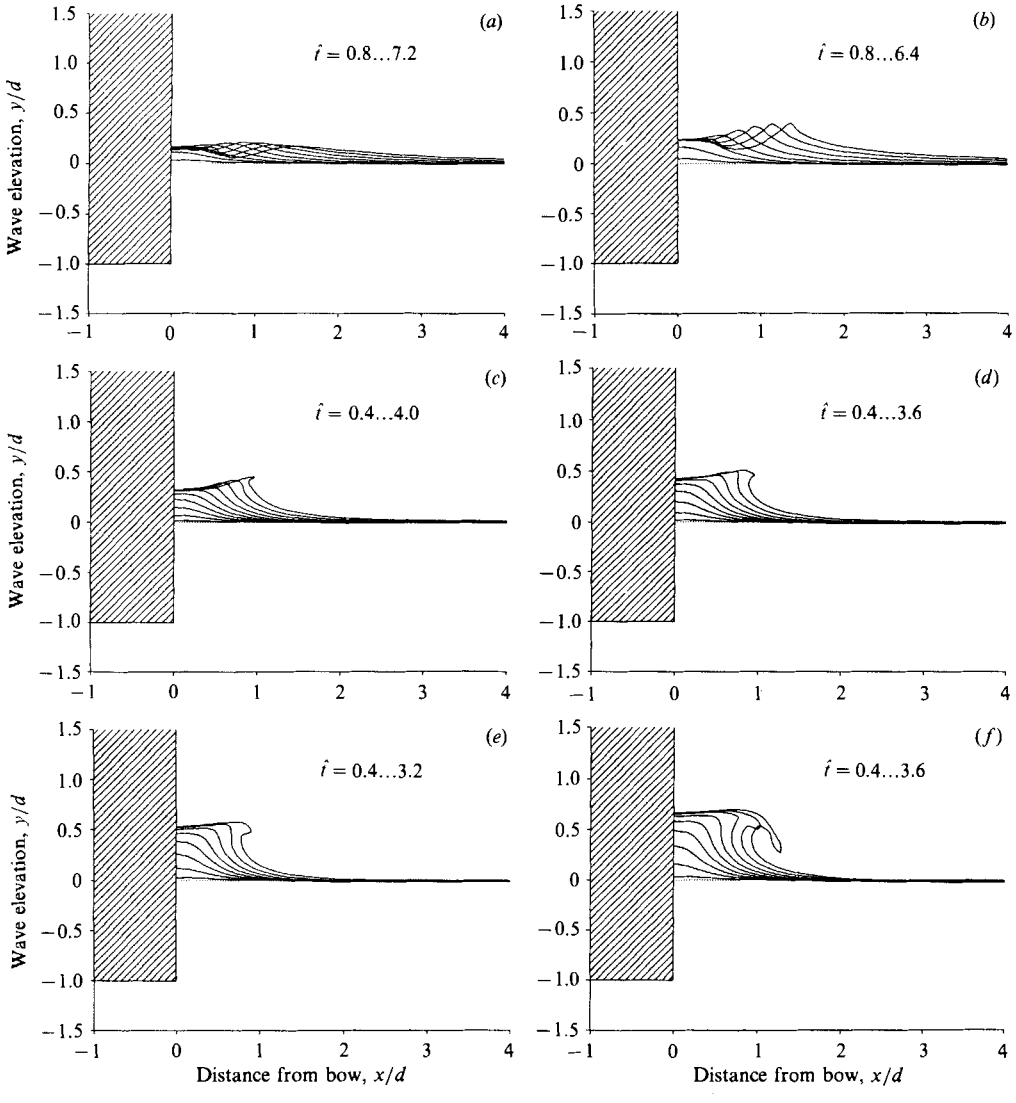

FIGURE 5. Bow-wave evolution for vertical step for Froude numbers $F_d = 0.5$ to 1.0. (a) $F_d = 0.5$; (b) 0.6; (c) 0.7; (d) 0.8; (e) 0.9; (f) 1.0.

The velocity field within the fluid domain was calculated using (3). For points on the boundary, (3) yields $w = \mathrm{d}\beta/\mathrm{d}z$ which can be obtained using central differencing. Figure 6 shows the instantaneous velocity field (as seen by an observer moving with the body) for $F_d = 0.5$. The individual frames are spaced at intervals of 0.8 time units. Figure 7 shows the instantaneous velocity field for $F_d = 1.0$. The individual frames in this case are spaced at intervals of 0.4 time units. The size of the arrows in both figures is scaled according to the magnitude of the flow velocity. Shown in each of the frames is the stagnation point, which is taken as the point at which the tangential velocity on the body vanishes.

The shape of the bow of the faired body is found by solving the equation

$$y = 0.3235 \tan^{-1}\left(\frac{y}{x+0.3235}\right). \tag{30}$$

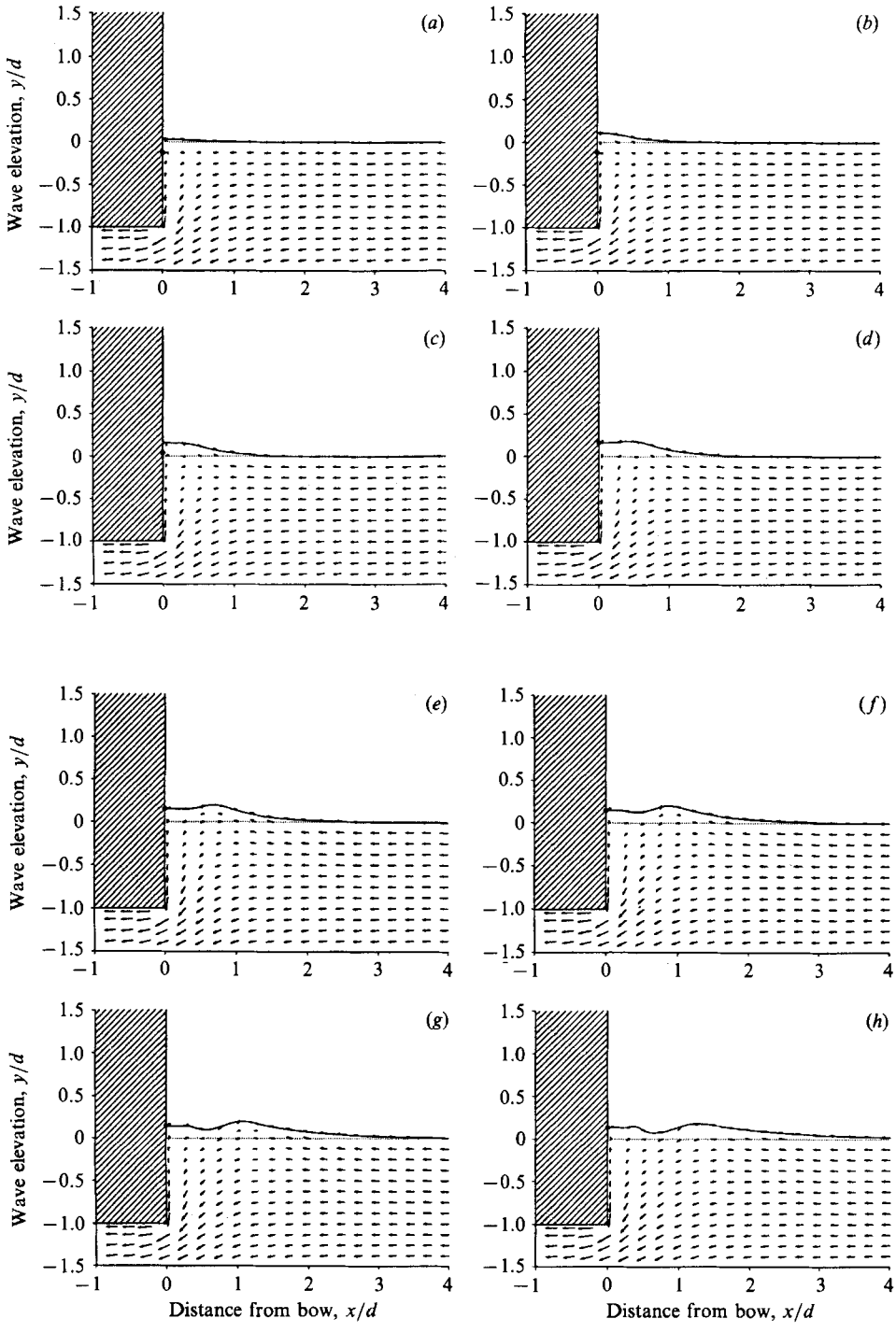

FIGURE 6. Instantaneous flow fields for vertical step, $F_d = 0.5$, for time (*a*) $\hat{t} = 0.8$; (*b*) 1.6; (*c*) 2.4; (*d*) 3.2; (*e*) 4.0; (*f*) 4.8; (*g*) 5.6; (*h*) 6.4. (Viewed in a coordinate system moving with the body.) •, Stagnation point.

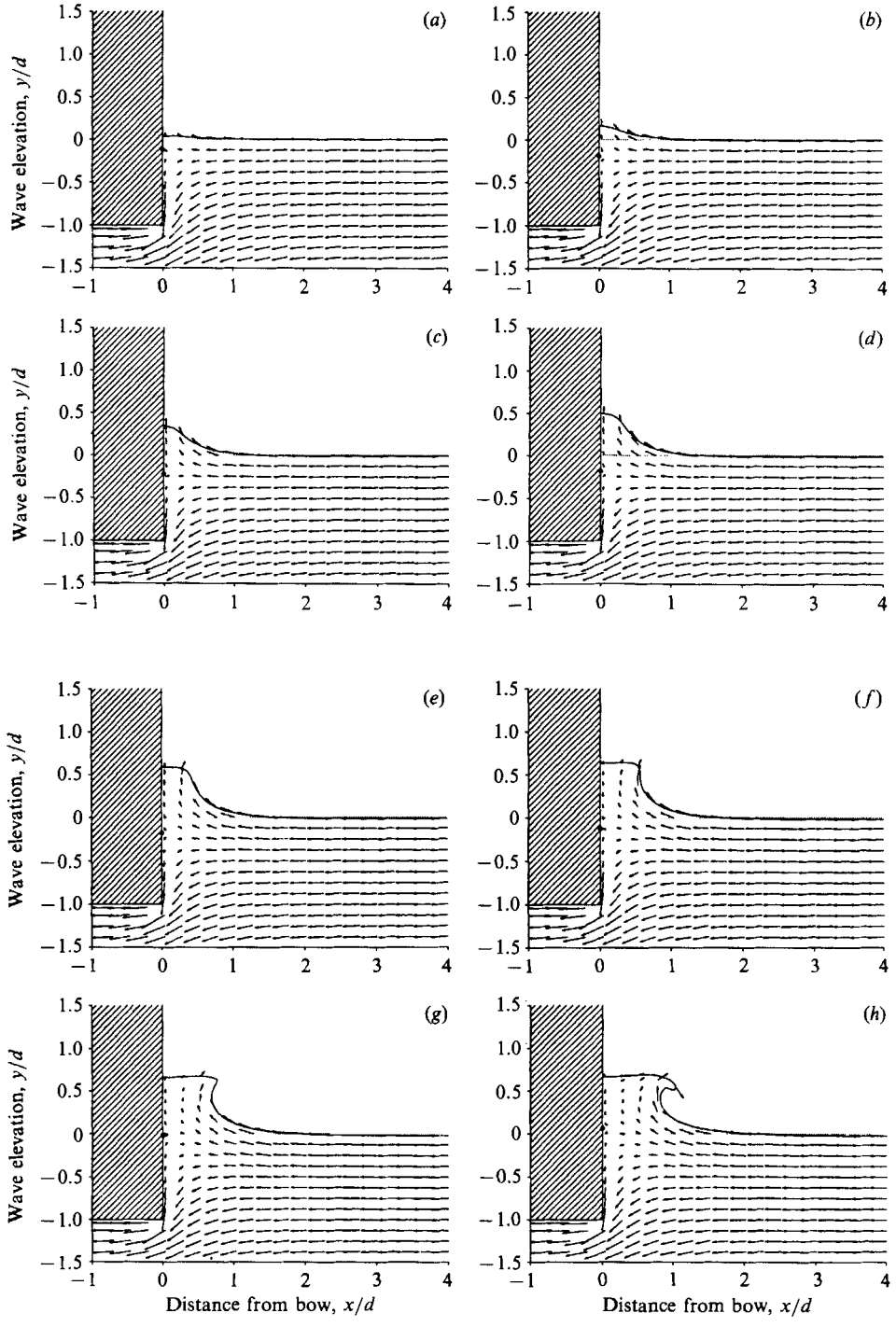

FIGURE 7. Instantaneous flow fields for vertical step, $F_d = 1.0$, for time (*a*) $\hat{t} = 0.4$; (*b*) 0.8; (*c*) 1.2; (*d*) 1.6; (*e*) 2.0; (*f*) 2.4; (*g*) 2.8; (*h*) 3.2. (Viewed in a coordinate system moving with the body.) •, Stagnation point.

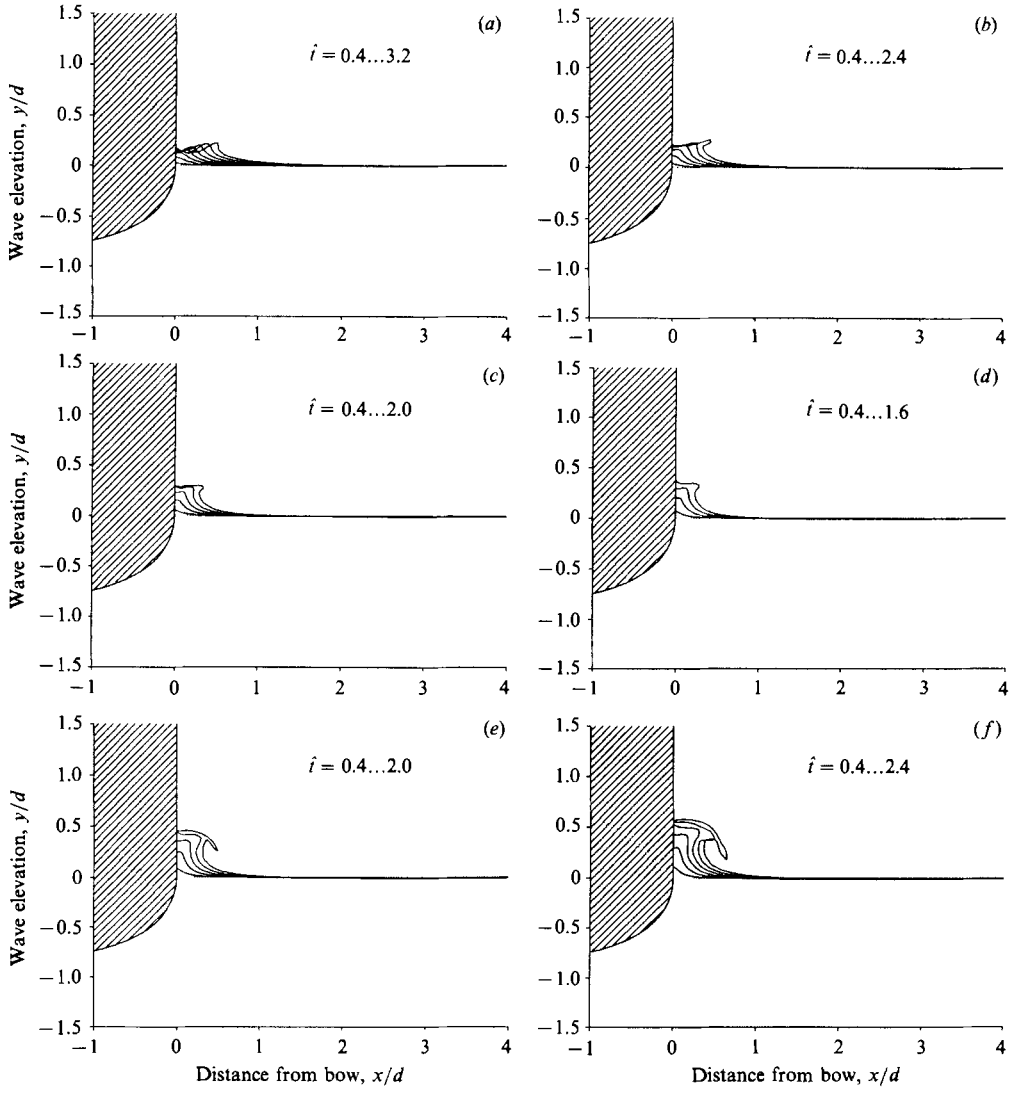

FIGURE 8. Bow-wave evolution for 'faired body' for Froude numbers $F_d = 0.5$ to 1.0. (*a*) $F_d = 0.5$; (*b*) 0.6; (*c*) 0.7; (*d*) 0.8; (*e*) 0.9; (*f*) 1.0.

This corresponds to the shape generated by placing a simple source in a uniform flow so that the stagnation point of the 'double-body' flow is at the origin and the draught of the body at $x = -\infty$ is 1.0. The initial conditions are given by

$$\beta(z, 0) = 0.3235 F_d \log(z + 0.3235). \tag{31}$$

The evolution of the free surface for Froude numbers $F_d = 0.5$ to $F_d = 1.0$ is shown in figure 8. The draught is measured at the point of intersection between the body and the downstream, far-field boundary. In each of the figures, the profiles are spaced at equal intervals of 0.4 time units. The time step for all the calculations was 0.01 time units.

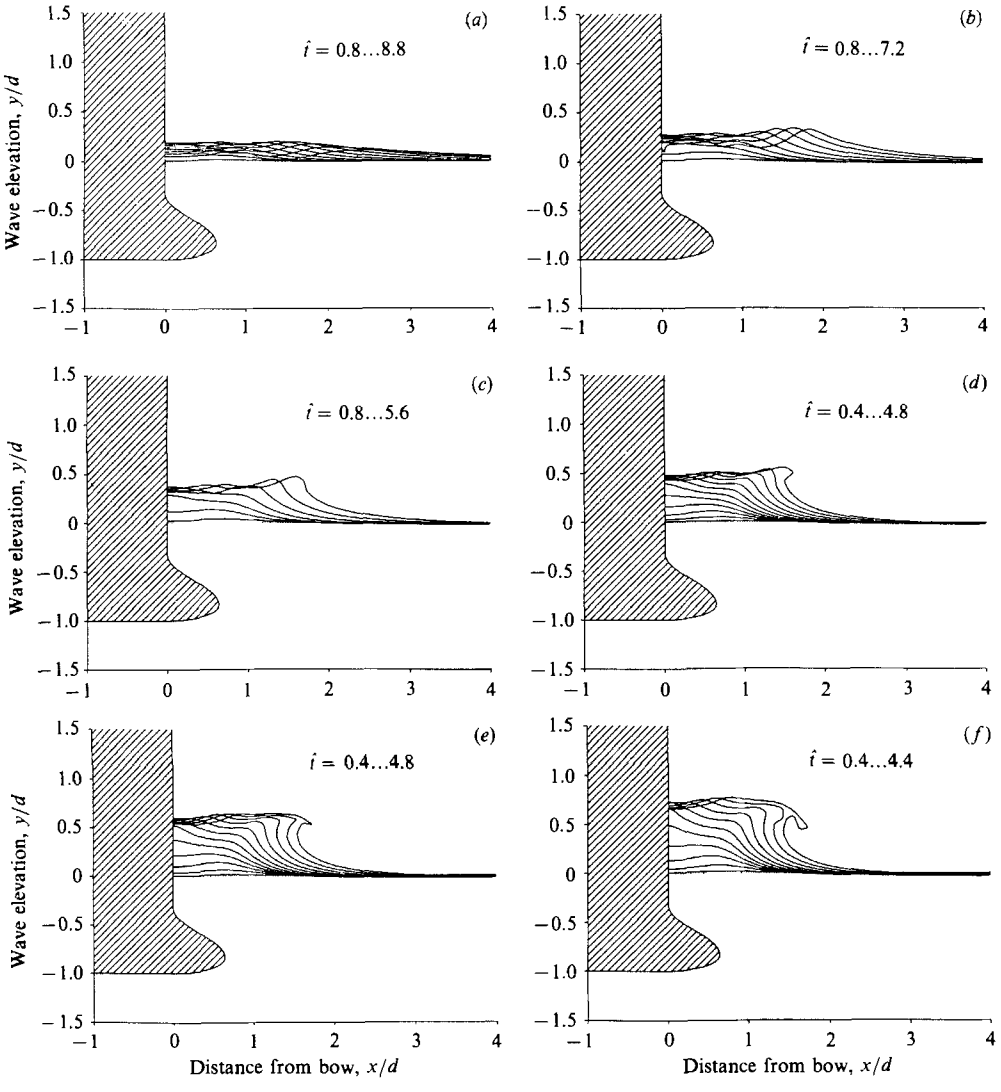

FIGURE 9. Bow-wave evolution for bulbous bow for Froude numbers $F_d = 0.5$ to 1.0. (a) $F_d = 0.5$; (b) 0.6; (c) 0.7; (d) 0.8; (e) 0.9; (f) 1.0.

The profile of the bulbous bow is given by the equation

$$x = \begin{cases} 0, & 0 \geqslant y \geqslant -0.32, \\ 0.32 \sin\left[\dfrac{(y+0.58)\,\pi}{0.52}\right] + 0.32, & -0.32 \geqslant y \geqslant -0.84, \\ 4[(0.16)^2 - (y+0.84)^2]^{\frac{1}{2}}, & -0.84 \geqslant y \geqslant -1. \end{cases} \tag{32}$$

Initial conditions for the potential ϕ were obtained by applying Green's theorem to a closed body that was 200 units long with a bulb at each end (Yeung 1975). We estimate that the difference between the values of the potential for this closed body and a semi-infinite body are at most $\frac{1}{2}\%$.

The evolution of the bow wave for the bulbous bow for Froude numbers $F_d = 0.5$

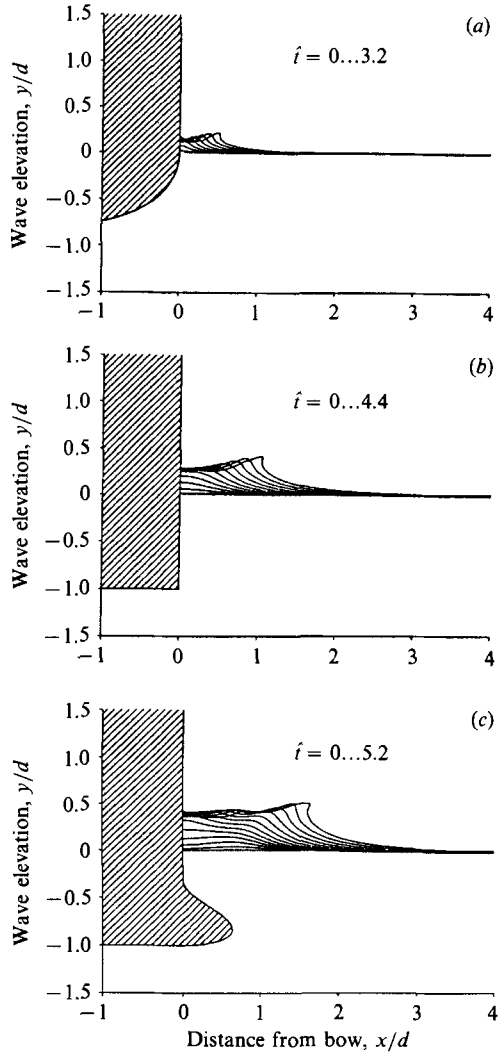

FIGURE 10. Comparison of the bow-wave evolution for the three geometries near the transition Froude number. (*a*) Faired body, $F_d = 0.5$; (*b*) vertical step, $F_d = 0.65$; (*c*) bulbous bow, $F_d = 0.74$.

to $F_d = 1.0$ are shown in figure 9. A time step of 0.01 time units was used for all the calculations. For $F_d = 0.5$ to $F_d = 0.7$, the bow wave profiles are plotted every 0.8 time units. The remaining wave profiles for $F_d = 0.8$ to $F_d = 1.0$ are plotted every 0.4 time units.

The existence of two different flow regimes is typical for all bow shapes studied here. At low Froude numbers a bow wave forms and travels upstream but does not overturn. The amplitude of this wave actually decays with time, and the slope just ahead of the wave becomes less steep. The long-time solution of this nonlinear problem is limited, however, by an inability to resolve waves of increasingly shorter wavelengths near the bow. Eventually, the formation and overturning of a second and shorter wave behind the main bow wave prevents the *calculation from* continuing.

For higher Froude numbers, the wavefront of the bow wave steepens and

overturns. The value of the Froude number above which overturning occurs is a function of the body shape. Let us define the transition Froude number as the lowest Froude number at which the wavefront of the bow wave becomes vertical. The transition for the vertical step occurred at approximately $F_d = 0.6$ (figure 5). For the faired body (figure 8) the transition was near $F_d = 0.5$. The body with the bulbous bow had a transition Froude number of approximately 0.7 (see figure 9).

It is noteworthy that the two distinct types of responses shown here are reminiscent of Tulin's (1982) classification of steady nonlinear waves behind a submerged body. He argued that weakly nonlinear and strongly nonlinear regimes exist. Thus, for sufficiently strong disturbances, steep wave elevations arise whose physical existence in a steady-state manner is questionable.

Tuck & Vanden-Broeck (1985) examined the *steady* free-surface flow about bodies with different shapes and attemped to find nonlinear solutions that would represent bow flow. They did this by calculating waveless *stern* flows! If they were successful then they could reverse the flow since a splashless bow would automatically satisfy the upstream radiation condition. Their study suggests the possible existence of splashless flows. They noted that the profile of the splashless bow has the shape of a protruding bow. In the present study, we showed that the bulbous bow had the favourable effect of delaying wave-breaking instability to a higher Froude number.

A simultaneous display of the bow-wave profiles at the transition Froude number for the three bodies (figure 10) shows their striking similarity. The similarity suggests a possible self-similar scaling in space and time (discussed further in Grosenbaugh 1987).

An important question that we hoped to address when we began this study was what are the nature and location of the stagnation point. In Dagan & Tulin (1972) and Vanden-Broeck & Tuck (1977) it was explicitly assumed that the stagnation point occurred at the intersection between the free surface and the body. In three-dimensional flow, Wehausen (1969) made an implicit assumption that there was a line of stagnation points along the bow stem when he formulated the wave resistance problem in Lagrangian coordinates. Hong (1977) used these results to predict the second-order wave resistance of different ship models. He found that good agreement with experimental data was limited to a narrow range of Froude numbers. The poor agreement outside of this range was attributed to the stagnation-point assumption. Fry & Kim (1984) used a three-component laser-Doppler velocimeter to determine experimentally the velocity field at the bow of ship models at draught Froude numbers $F_d = 1.06$ to 1.96. They were able to identify an isolated stagnation point located beneath the free surface for the models with bulbous bows.

The present study indicates that there exists an isolated stagnation point which behaves differently for the breaking and non-breaking flow regimes. As can be seen from figure 7, the stagnation point of the calculated flow at $F_d = 1.0$ for a vertical step is located below the free surface and remains there as the wave overturns. For $F_d = 0.5$ (see figure 6), the stagnation point initially drops below the free surface but then returns to the surface. Similar behaviour was also observed for the other two geometries. The vertical locations of the stagnation point are plotted as a function of time in figure 11 for all three bow shapes. Figure 11 (*a*) corresponds to flow in the non-breaking regime ($F_d = 0.5$). Figure 11 (*b*) shows the behaviour for flow in the breaking regime ($F_d = 1.0$). The curves represent the free-surface elevation at the bow, and the open symbols correspond to the location of stagnation point.

We believe that for sufficiently low Froude numbers, calculations with accurate

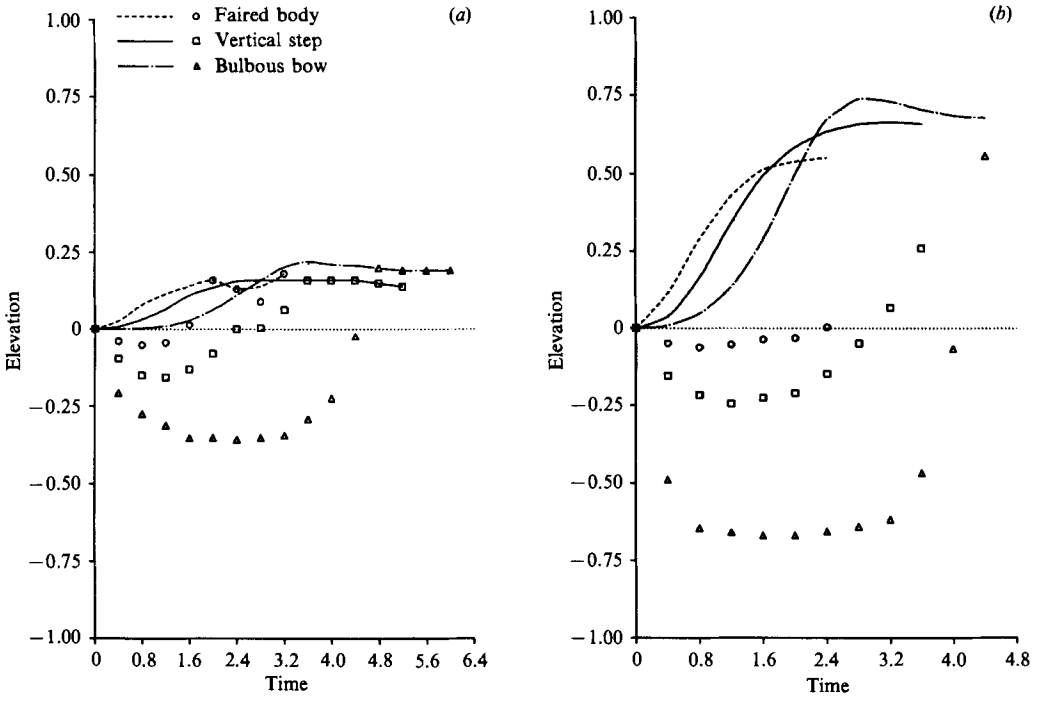

FIGURE 11. Free-surface elevation at the bow (curves) and location of stagnation point (symbols) plotted versus time for (*a*) $F_d = 0.5$ and (*b*) $F_d = 1.0$.

spatial resolution would approach steady-state conditions. This may be inferred by examining the profiles of all the bow shapes at Froude numbers below the transition value. The amplitude of the bow wave decays with time, the stagnation point returns to the free surface, and the free-surface elevation at the body settles near the stagnation height of $\frac{1}{2}F_d^2$ (see figure 11*a*). The reason that we were not able to reach steady state was that waves of higher and higher wavenumbers formed at the bow. Thus, no matter how small the grid, there would always be a wave that could not be resolved by the calculation.

6. Conclusion

A mixed Eulerian–Lagrangian method is used to solve the unsteady flow around a semi-infinite body. The novelty in the approach is in the choice of initial and far-field boundary conditions. An inviscid 'double-body' solution is taken as the initial condition. It is argued that this can be a realistic condition to use in calculating the unsteady flow of a body that has been moving for a long time. The alternative of setting the potential in the fluid equal to zero at $t = 0$ and starting the body from rest is more reasonable for studying impulsive motion.

Lagrangian marker particles are distributed on both the free surface and the far-field boundary. Evolution equations, describing how the particles move and how their potential changes, are derived for the points on the far-field boundary. The evolution equation for the potential is exact for particles on the free surface; it is approximate on the far-field boundary. The pressure of the far-field particles is kept

constant with time. It is shown that this assumption gives an error which varies inversely with the distance from the body. Calculations using this method were found to give a relative error in energy of less than 5%. This error does not accumulate.

Solutions were obtained over a range of Froude numbers for three different body shapes: a vertical step, a faired profile, and a bulbous bow. For all three, there exists a transition Froude number at which the bow wave begins to overturn and break. The value of the transition Froude number varies with bow shape. The fuller the profile geometry, the larger is the value. Thus, the bulbous bow delays wave breaking.

For all cases studied, an isolated stagnation point located below the free surface occurs during the initial stage of the wave formation. If the Froude number is above the transition value, the stagnation point remains trapped below the free surface as the wave overturns. Below the transition Froude number, the stagnation point rises to the surface as the crest of the bow wave moves upstream, and away from the body. These calculations suggest that, at sufficiently low Froude numbers, the flow can reach a steady-state condition with the stagnation point located at the free surface.

The research and preparation of this paper has been supported by the Office of Naval Research under contracts N00014-84-K0026 and N00014-88-K0002.

REFERENCES

BABA, E. 1969 A new component of viscous resistance of ships. *J. Soc. Naval Archit. Japan* **125**, 23–34.

BAKER, G. B., MEIRON, D. I. & ORSZAG, S. A. 1982 Generalized vortex method for free-surface flow problems. *J. Fluid Mech.* **123**, 477–501.

DAGAN, G. & TULIN, M. P. 1972 Two-dimensional free-surface gravity flow past blunt bodies. *J. Fluid Mech.* **51**, 529–543.

DOMMERMUTH, D. G. & YUE, D. K. 1986 Study of nonlinear axisymmetric body–wave interactions. *Proc. 16th Symp. on Naval Hydrodynamics, Berkeley, California*, pp. 116–126.

FINKELSTEIN, A. B. 1957 The initial value problem for transient water waves. *Commun. Pure Appl. Maths* **10**, 511–522.

FRY, D. J. & KIM, Y. H. 1984 Bow flow field of surface ships. *Proc. 15th Symp. on Naval Hydrodynamics, Hamburg, W. Germany*, pp. 319–345.

GROSENBAUGH, M. A. 1987 Nonlinear flow at the bow of a ship: an experimental and theoretical investigation. Ph.D. dissertation, Dept. of Naval Archit. and Offshore Engng, U. of California, Berkeley.

HILDEBRAND, F. B. 1976 *Calculus for Applications*. Prentice-Hall.

HONG, Y. S. 1977 Numerical calculation of second-order wave resistance. *J. Ship Res.* **21**, no. 2, pp. 94–106.

JOHN, F. 1949 On the motion of floating bodies – I. *Commun. Pure Appl. Maths* **2**, 13–57.

LIN, W. M., NEWMAN, J. N. & YUE, D. K. 1984 Nonlinear forced motion of floating bodies. *Proc. 15th Symp. on Naval Hydrodynamics, Hamburg, W. Germany*, pp. 33–47.

LONGUET-HIGGINS, M. S. & COKELET, E. D. 1976 The deformation of steep surface waves on water. I. A numerical method of computation. *Proc. R. Soc. Lond.* A **350**, 1–26.

MIYATA, H., SUZUKI, A. & KAJITANI, H. 1981 Numerical explanation of nonlinear nondispersive waves around bow. *Proc. 3rd Intl Conf. Numerical Ship Hydrodynamics, Paris, France*, pp. 37–54.

MORI, K. 1984 Necklace vortex and bow wave around blunt bodies. *Proc. 15th Symp. on Naval Hydrodynamics, Hamburg, W. Germany*, pp. 9–20.

OGILVIE, T. F. 1968 Wave resistance: the low speed limit. *University of Mich., College of Engng Rep. 002, Dept. of Nav. Archit. and Marine Engng.*

ROBERTS, A. J. 1987 Transient free-surface flows generated by a moving vertical plate. *Q. J. Mech. Appl. Maths* **40**, 129–158.

TUCK, E. O. & VANDEN-BROECK, J. M. 1984 Splashless bow flows in two dimensions. *Proc. 15th Symp. on Naval Hydrodynamics, Hamburg, W. Germany*, pp. 293–300.

TULIN, M. P. 1982 An exact theory of gravity wave generation by moving bodies, its approximation, and its implications. *Proc. 14th Symp. on Naval Hydrodynamics, Ann Arbor, Mich.*, pp. 19–48.

VANDEN-BROECK, J.-M., SCHWARTZ, L. W. & TUCK, E. O. 1978 Divergent low-Froude-number series expansions of nonlinear free-surface flow problems. *Proc. R. Soc. Lond.* A **361**, 207–224.

VANDEN-BROECK, J.-M. & TUCK, E. O. 1977 Computations of near-bow and stern flows using series expansions in the Froude number. *Proc. 2nd Intl Conf. on Numerical Ship Hydrodynamics, Berkeley, California*, pp. 377–387.

VINJE, T. & BREVIG, P. 1981 Nonlinear ship motions. *Proc. 3rd Intl Conf. Numerical Ship Hydrodynamics, Paris, France*, pp. 257–268.

WEHAUSEN, J. V. 1969 Use of Lagrangian coordinates for ship wave resistance (first- and second-order thin-ship theory). *J. Ship Res.* **12**, 12–22.

YEUNG, R. W. 1975 A hybrid integral-equation method for time-harmonic free-surface flows. *Proc. 1st Intl Conf. Numerical Ship Hydrodynamics, Gaithersburg, Maryland*, pp. 581–608.

YEUNG, R. W. 1982 Numerical methods in free-surface flows. *Ann. Rev. Fluid Mech.* **14**, 395–442.